



OPEN

Fullerene Embedded Shape Memory
Nanolens ArraySohee Jeon^{1*}, Jun Young Jang^{2*}, Jae Ryoun Youn^{1*}, Jun-ho Jeong³, Howard Brenner⁴ & Young Seok Song²

¹Research Institute of Advanced Materials (RIAM), Department of Materials Science and Engineering, Seoul National University, Daehak-Dong, Gwanak-Gu, Seoul 151-744, Korea, ²Department of Fiber System Engineering, Dankook University, 126 Jukjeon-dong, Suji-gu, Yongin-si, Gyeonggi-do 448-701, Korea, ³Department of Nano Manufacturing Technology, Intelligent and Precision Machinery Research Division, Korea Institute of Machinery and Materials, 104 Sinseongno, Yuseong-gu, Daejeon, 305-343, Republic of Korea, ⁴Department of Chemical Engineering, Massachusetts Institute of Technology, Cambridge, Massachusetts 02139, USA.

Received
29 May 2013Accepted
31 October 2013Published
20 November 2013Correspondence and
requests for materials
should be addressed to
Y.S.S. (ysong@
dankook.ac.kr)* These authors
contributed equally to
this work.

Securing fragile nanostructures against external impact is indispensable for offering sufficiently long lifetime in service to nanoengineering products, especially when coming in contact with other substances. Indeed, this problem still remains a challenging task, which may be resolved with the help of smart materials such as shape memory and self-healing materials. Here, we demonstrate a shape memory nanostructure that can recover its shape by absorbing electromagnetic energy. Fullerenes were embedded into the fabricated nanolens array. Beside the energy absorption, such addition enables a remarkable enhancement in mechanical properties of shape memory polymer. The shape memory nanolens was numerically modeled to impart more in-depth understanding on the physics regarding shape recovery behavior of the fabricated nanolens. We anticipate that our strategy of combining the shape memory property with the microwave irradiation feature can provide a new pathway for nanostructured systems able to ensure a long-term durability.

Enormous effort has been made to fabricate nanostructures for a wide range of applications, such as optical^{1,2}, biological³, electrical⁴, mechanical⁵, thermal^{6,7}, and chemical⁸ areas due to their exceptionally superior physical features. Indeed, materials at nanoscale are allowed to reveal their own intrinsic, extraordinary properties. However, nanostructure is susceptible to damage by external impact, which is a must-resolve durability issue for practical application. In this respect, smart materials responding to specific stimuli, especially shape memory materials may act as a solution to such a matter. Shape memory materials are generally classified into shape memory alloy (SMA) and shape memory polymer (SMP). SMPs which are recovered by entropy change in their long and intertwined molecular chains have advantages over SMAs, such as low specific weight, good processability, low cost, and large recovery strain (up to 800%)⁹. However, their major shortcoming is relatively low recovery stress induced by poor mechanical properties such as hardness and Young's modulus (e.g., 1 ~ 3 MPa for SMPs versus 200 ~ 500 MPa for SMAs)¹⁰.

Herein, we introduce a new material system that is designed for overcoming the existing weakness of nanopattern, i.e., low durability by embedding fullerenes into SMPs. It is known that carbon nanotubes (CNTs) are heated by microwave irradiation through transformation of electromagnetic energy into mechanical vibration¹¹. In a similar manner, fullerene, also called a buckyball, absorbs electromagnetic waves such as UV and microwave and then emits heat toward surroundings due to its resonant responses to the wave entailing electron-phonon scattering and phonon-phonon scattering³. Besides, fullerenes can offer good mechanical and electrical properties to material systems. Such a thermophysical mechanism can serve as an energy source for the transition between frozen and active phases of SMPs at transition temperature, T_{tr} when fullerenes are incorporated in SMPs.

Results

One of the biggest uses of nanostructured patterns is for optical application. For this reason, we constructed a nanolens array with fullerene reinforced SMPs (Fig. 1a). The nanostructure was fabricated using nanoimprint lithography. Fullerenes with a diameter of 1 nm were dispersed in Polynorbornene solution before the resulting suspension was cast onto the nanopatterned silicon template fabricated via photolithography. C_{60} fullerenes, which have large energy gaps between the highest occupied and lowest unoccupied molecular orbitals (HOMO and LUMO), are soluble in many organic solvents. After preparing the fullerene/SMP layer, an additional PMMA

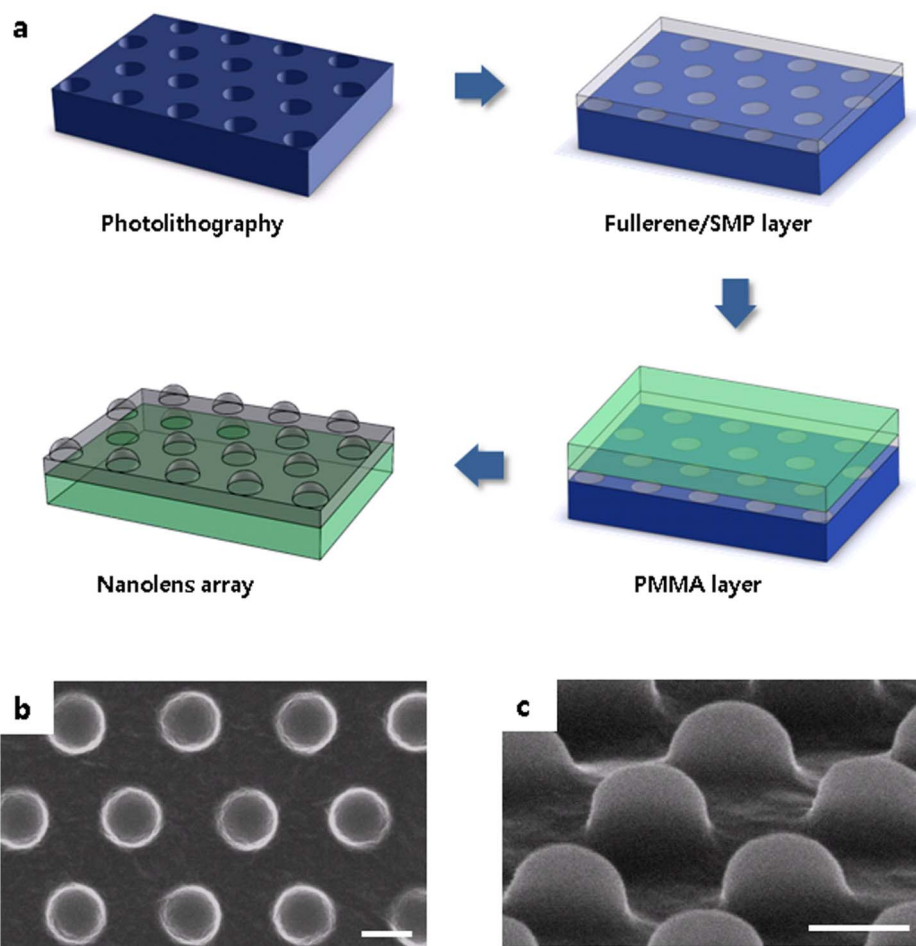


Figure 1 | Fullerene embedded nanolens array. (a), Schematic diagram of preparation procedure for the nanolens array. Nanostructure is generated on the silicon template using photolithography. The SMP solution, where fullerenes are suspended, is cast on the nanopatterned template. In addition, a PMMA layer is fabricated, followed by detaching the nanolens array from the silicon template. (b), (c), SEM images of the nanolens array ((b) top view and (c) tilt view). The scale bars indicate 200 nm.

layer was fabricated in an effort to give more stable dimensionality to the nanostructure. As shown in Fig. 1b and 1c, a nanolens array structure was formed.

We characterized the thermophysical features of fullerene embedded SMPs. Fig. 2a presents the energy absorption behavior from a microwave frequency electromagnetic field. The drastic increase in temperature was observed for the SMPs containing 0.1 wt% fullerene compared with the control sample without fullerene. In general, electromagnetic absorption relies upon the complex permeability (μ_r), complex permittivity (ϵ_r), electromagnetic impedance match of materials, and nanosized structures¹². It has been reported that the addition of as little as 0.04 wt% carbon nanotubes yields dramatic enhancement of microwave absorbance by 500 times¹³. Basically, SMPs are composed of two different phases, i.e., frozen phase and reversible phase. The frozen phase with a higher thermal transition temperature ($T_{tr} = T_{perm}$) acts as a physical crosslink maintaining permanent shape, while the reversible phase with a lower phase transition temperature ($T_{tr} = T_g$ or T_m) plays the role of a ‘molecular switch’ fixating temporary shape^{14,15}. The microwave heating can reach the glass transition temperature ($\sim 37^\circ\text{C}$) of Polynorborene. The incorporation of particles into SMPs enables one to introduce fascinating characteristics, such as high thermal and electrical conductivities, magnetic- and moisture-responsive behavior, and superior mechanical properties^{9,16–18}. For instance, the SMP composites filled with either carbon powders¹⁹ or SiC particles²⁰ yield enhanced mechanical

properties such as recovery stress and Young’s modulus. Interestingly, embedding fullerene into SMPs allows us to bring in two different effects, light-response feature and reinforcement at the same time.

Significant improvement of mechanical properties for fullerene reinforced SMPs was detected from the nanoindentation experiment (Fig. 2b) and the tensile test (Supplementary Fig. S11 and Table S1). In particular, the addition of fullerene led to a remarkable increase in Young’s modulus of the composite by more than ten times (i.e., from 124 MPa to 1290 MPa). Furthermore, the tensile strength and hardness of the specimen were significantly enhanced by incorporating fullerene into SMPs. It turned out that fullerene played a role in absorbing microwaves and reinforcing materials successfully.

The fabricated nanolens array is demonstrated in Fig. 3a. The array was deformed by pressing with a finger (Fig. 3b). The severely deformed nanostructure was recovered with the help of microwave irradiation (Fig. 3c). For more quantitative validation, atomic force microscopy analysis was conducted (the insets in Fig. 3a, b, and c). In this study, a new quantity, shape recovery ratio (R_s) was proposed to describe the shape memory effect at nanoscale. A shape recovery ratio of 97.6% was obtained based on the height of the nanolenses. In addition, the strain recovery rate (R_r) and the strain fixity rate (R_f) were measured to characterize the abilities of memorizing a permanent shape and fixing a strain given to the sample, respectively. More details are presented in Supplementary Information.

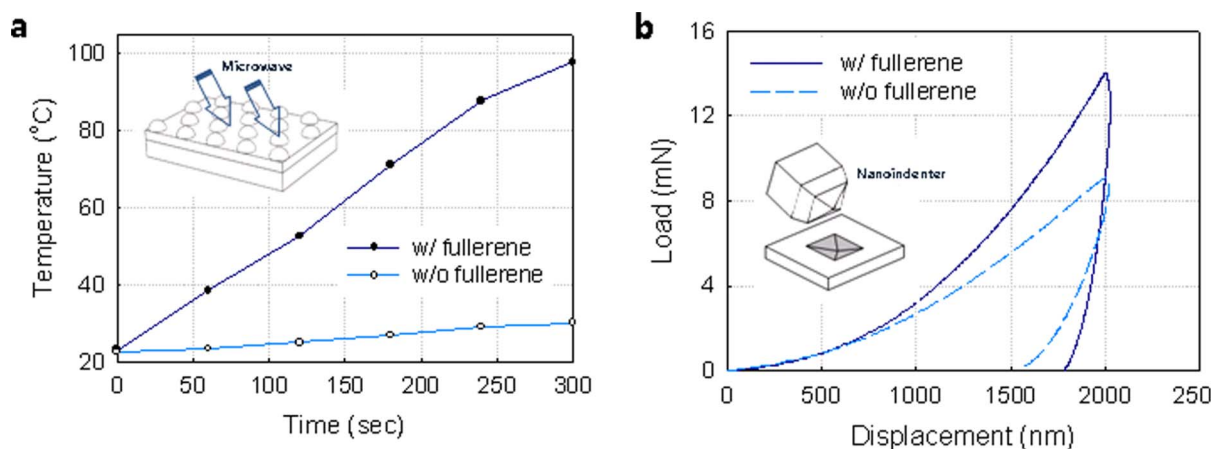


Figure 2 | Thermophysical and mechanical behavior of the nanolens array. (a), Temperature versus time for the nanolens array with and without fullerenes. The nanostructure absorbs electromagnetic wave, which is as a result of the embedded fullerenes in the SMP. Such an increment in temperature is high enough to reach the transition temperature of SMPs. (b), Load versus displacement for the nanolens array with and without fullerenes. The results are obtained via the nanoindentation experiment. The fullerene reinforced nanostructure provides the enhanced load-displacement relation compared with the specimen without fullerenes.

We identified the shape recovery behavior of the nanostructure made of fullerene embedded SMPs. Thus far, the recovery property of shape memory materials has been stressed mainly at macroscale. To the best of our knowledge, this is the first report to apply the shape memory feature to the nanoscale structure. The thermomechanical cycle of the shape memory material consists of the programming and recovery processes (Supplementary Fig. S1). In the programming process, SMP is deformed from its permanent shape to temporary shape at a high temperature and then cooled down. On the other hand, the recovery process is conducted by heating SMP above a transition temperature. This is the so-called one-way shape memory effect.

To understand the underlying physics of the shape memory behavior, we carried out thermomechanical constitutive modeling²¹. In general, two approaches have been adopted to describe the thermo-mechanical behavior of SMPs²²; one is a linear viscoelastic model²³ and the other a micromechanical model based on phase transition²⁴.

Since the micromechanical model implemented in this study utilizes internal state variables and molecular mechanism of SMPs, it can predict strain storage and recovery behaviors using the calculated correlation among stress, strain, and temperature. More details regarding the constitutive modeling are presented in Supplementary Information. The simulation results demonstrate that the nanolens completely recovers its initial shape through the reversible transition between permanent and temporary shapes (Fig. 3d, e, and f). This stress-free strain recovery is induced by the thermomechanical cycle of stress, strain, and temperature (Supplementary Fig. S1). In addition, the model predictions successfully describe the deformation and recovery of the nanostructure on the nanoscale.

Compared with other nanostructured arrays such as nanorods²⁵, nanocones²⁶, and nanodomes²⁷, nanolens array has relatively high optical transmittance, which can provide superior power or light generation in optical devices^{28,29}. The optical behavior of initial, deformed, and recovered nanostructures are compared in terms of

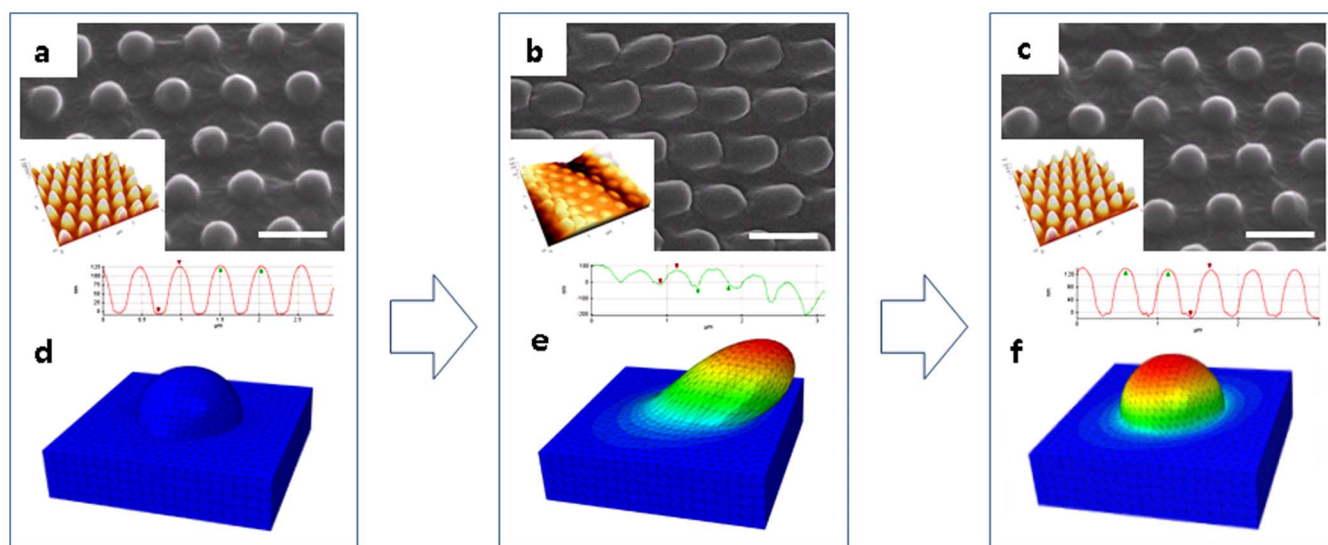


Figure 3 | Shape Recovery Characteristics of nanolens array. (a), (b), (c), SEM images of the nanolens array ((a) initial, (b) deformed, and (c) recovered states). The nanostructure is deformed by an external force. After then, the microwave is irradiated on the nanolens array, thus recovering its original shape. The scale bars indicate 500 nm. AFM analyses for the nanolens array are carried out (the insets). The shape recovery behavior of the nanolens array is identified in a quantitative manner (shape recovery ratio of 97.6%). (d), (e), (f), Finite element analyses for the shape memory nanolens array ((h) initial, (i) deformed, and (k) recovered states). The modeling is performed using the thermomechanical cycle of stress, strain, and temperature.

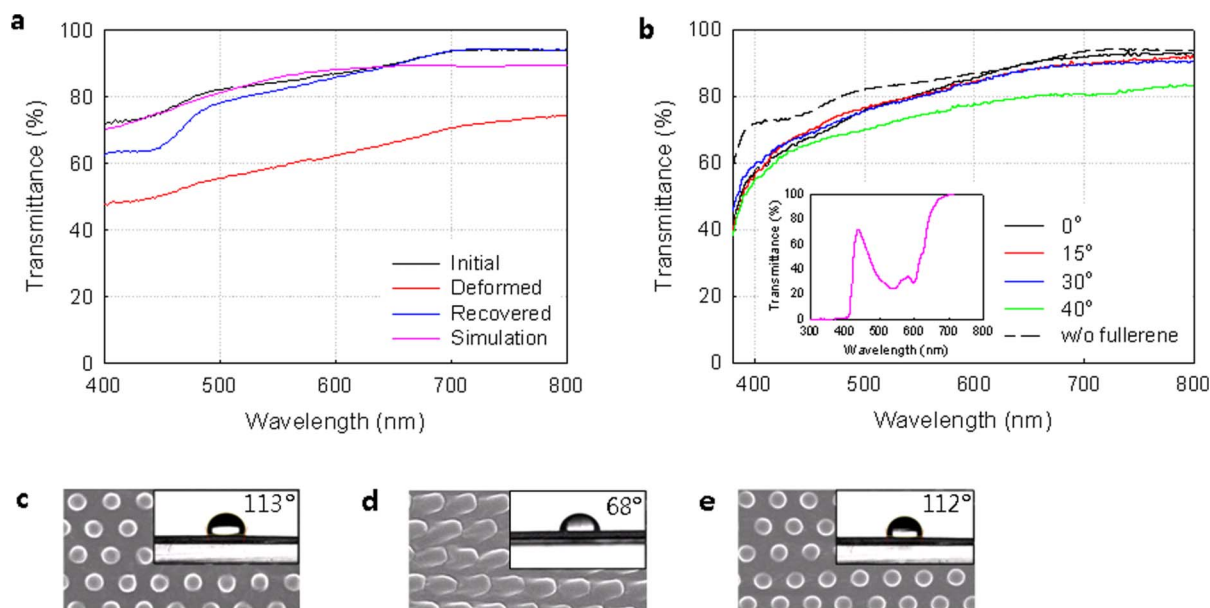


Figure 4 | **Optical and surface characterizations of the nanolens array.** (a), Transmittance versus wavelength of the nanolens array. The initial, deformed, and recovered nanostructures are compared in terms of transmittance. It turns out that the nanolens array is optically recovered as a result of the absorption of electromagnetic energy. In addition, the numerical simulation result obtained from FDTD is compared with the experimental results. (b), Transmittance versus wavelength of the nanolens array. The transmittance changes according to the angle of the incident light. The transmittance remains nearly at the same level up to 30° inclination. There is a significant difference between the transmittances for the specimens with and without fullerenes due to the electromagnetic wave absorption of fullerenes as shown in the inset. (c), (d), (e), Contact angle variation of the nanolens array ((d) initial, (e) deformed, and (f) recovered states). The contact angle starts with 113°, decreases down to 68°, and returns to 112°.

transmittance with respect to wavelength (Fig. 4a). Similar to the mechanical recovery behavior aforementioned, the nanolens array is optically recovered by means of microwave irradiation. The distinction between the transmittance values of the deformed and recovered nanolens arrays is quite big, which suggests that the shape recovery nature can yield distinguished output in optical applications. The repeatability of the experimental results is presented in Supplementary Fig. S8. For the sake of validation, the computational electrostatics of the nanolens array is modeled using the finite-difference time-domain (FDTD) method (Fig. 4a). Both the simulation and experiment results reveal that the nanostructure not only suppresses reflectance but also traps more photons from incident light. The interaction between the incident light and the nanolens decreases with shifting to the long-wave regime, and incident light with a long wavelength can penetrate the nanostructure more readily. This is attributed to the fact that the transmittance increases with an increase in the wavelength. Fig. 4b displays the effect of the presence/absence of the nanolens on the transmittance (Supplementary Fig. S9). The existence of the nanostructure is of importance to decrease reduction in the transmittance with inclining the specimen, especially at 40°. Indeed, with help of the nanostructure, the transmittance through the nanopattern can remain nearly at the same level up to 30° inclination, which is critical for practical applications, such as solar cells due to its advantage in harvesting incident sunlight. Since fullerenes absorb electromagnetic wave (the inset of Fig. 4b), the fullerene embedded nanolens array exhibits slightly decreased transmittance compared with the nanolens without fullerene.

Additional investigation into the recovery behavior of the nanolens array is carried out by analyzing the contact angle (Fig. 4d–f). Depending on the thermomechanical cycles of the specimen, the contact angle changes from 113°, 68°, through 112° for initial, deformed, and recovered states, respectively. Considering the shape recovery ratio (97.6%) mentioned before, the recovery ratio of the

contact angle is found to be significantly enhanced. The relevant repeatability results are illustrated in Supplementary Fig. S13.

From a practical perspective, one of the key requirements for nanolenses is a low surface energy that can enhance the contact angle (CA) of solid surface³⁰. A self-cleaning nature of nanostructure is embodied by achieving low contact angle hysteresis (CAH) rather than a large CA since the former is a driving force for removing a liquid droplet⁵. For further understanding on the contact angle phenomenon, thermodynamic analysis including free energy (FE) and free energy barrier (FEB) of a metastable wetting state is conducted for verifying the experimental results (Fig. 5a). Two extreme cases, the noncomposite Wenzel state and the composite Cassie state, are simulated through the thermodynamic approach proposed in the current study. The normalized free energy result shows that the Wenzel and Cassie states have the minimum free energies at angles of 82° and 138°, respectively, and that the contact angle (113°) measured experimentally is in between those angles (Fig. 5b). This indicates that the surface state can be described by a combination of the Wenzel and Cassie systems. Depending on the arc angle of the nanolens α (or the arc length), the normalized free energy of the Wenzel state varies (Fig. 5c). In other words, the higher arc angle leads to the lower contact angle. CAH can be characterized by the distinction between the contact angles of advancing and receding droplets from one metastable state to another. Assuming a zero vibrational energy, the Cassie state provides a much larger CAH (i.e., the difference between an advancing angle of 176° and a receding angle of 82°) than the Wenzel state (Fig. 5d). Also, the normalized free energy barrier is analyzed according to the arc angle (Fig. 5e).

Discussion

We demonstrated the shape memory nanolens array that contains fullerenes not only to absorb electromagnetic energy but also to reinforce the nanostructure. In particular, Young's modulus of the

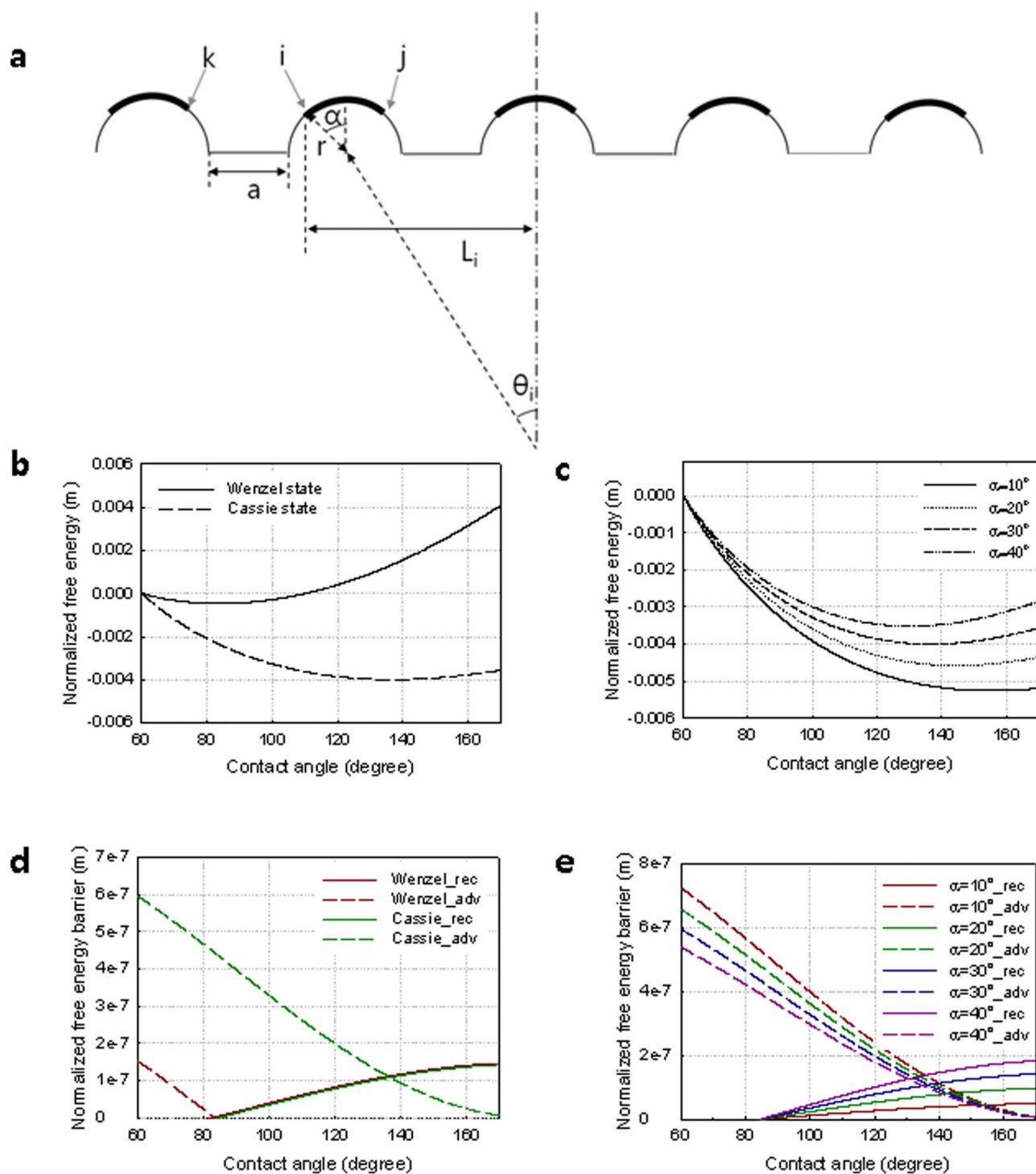


Figure 5 | Contact angle analyses of the nanolens array. (a), Schematic illustration of the nanolens array structure for theoretical calculation. The bold line indicates the contact between the nanolens and a liquid droplet. The resulting contact angle is obtained through thermodynamic analysis. In addition, advancing ($i \rightarrow k$) and receding ($i \rightarrow j$) cases are taken into account to obtain the lowest surface energy. (b), Normalized free energy (FE) versus contact angle. The composite (Cassie) and noncomposite (Wenzel) wetting states are considered in the calculation. The Wenzel and Cassie states show the minimum free energies at angles of 82° and 138° , respectively. (c), Normalized free energy of the nanolens array. The normalized FE decreases with increasing the arc angle of the nanolens. (d), Normalized receding and advancing free energy barrier (FEM) versus contact angle. The Cassie state has much bigger CAH than the Wenzel state. (e), Normalized free energy barrier (FEM) analyzed according to the arc angle.

composite was enhanced by more than ten times by incorporating fullerene into SMPs. The shape recovery behavior, optical properties, and contact angle of the nanolens array were investigated numerically and experimentally. We foresee that this material sys-

tem can be employed for manifold functional applications ranging from passive actuators and sensors, adaptive optical devices, and energy devices to surface engineering applications such as coating and tribology.



Methods

Sample preparation. Norsorex (Polynorbornene) selected as a shape memory polymer was obtained from Astrotech (Supplementary Fig. S2 a), and pristine fullerenes were purchased from Sigma Aldrich (Supplementary Fig. S2 b). All other chemicals were supplied by Fisher.

A silicon mold was fabricated for nanoimprinting using photolithography (Supplementary Fig. S3a). Prior to running experiments, the mold was treated with trichlorosilane at 80 °C for 4 hours for imposing hydrophobicity on the surface. Toluene was used as a solvent for Polynorbornene and Poly(methyl methacrylate) (PMMA). Fullerenes were dispersed in toluene for 30 min with the use of sonication, and then SMP was added in the suspension at 125 °C.

Modeling. Numerical analysis on the thermomechanical behavior of nanolens array was carried out. The constitutive model for SMPs was implemented using the nonlinear finite element software ABAQUS/Standard in conjunction with a user-defined subroutine (UMAT) and C3D8HT thermo-mechanically-coupled elements. For optical simulation, the finite difference time domain (FDTD) method was used to consider the interaction between incident light and nanolens array applying the periodic boundary condition in plane and the perfectly matched layer (PML) boundary condition out of plane (Supplementary Fig. S7).

Contact angle phenomena were investigated through thermodynamic analysis. For the composite state, the corresponding geometrical relation and free energy differences are expressed as follows:

$$(i) \theta_i \frac{L_i^2}{\sin^2 \theta_i} - L_i^2 \cot \theta_i - r^2 + r^2 \sin \alpha \cos \alpha = \theta_j \frac{L_j^2}{\sin^2 \theta_j} - L_j^2 \cot \theta_j,$$

$$(ii) \Delta F_{i \rightarrow j} / \gamma = \left(\theta_j \frac{L_j}{\sin \theta_j} - \theta_i \frac{L_i}{\sin \theta_i} \right) + 2rz \cos \theta_j,$$

$$(iii) \theta_i \frac{L_i^2}{\sin^2 \theta_i} - L_i^2 \cot \theta_i = \theta_k \frac{L_k^2}{\sin^2 \theta_k} - L_k^2 \cot \theta_k,$$

and

$$(iv) \Delta F_{i \rightarrow k} / \gamma = \left(\theta_k \frac{L_k}{\sin \theta_k} - \theta_i \frac{L_i}{\sin \theta_i} \right) - a - 2(r - r \sin \alpha),$$

where γ is the liquid surface tension, F is the FE, and θ_j is the intrinsic CA. The other equations for the noncomposite state are given in Supplementary Information. Those equations were calculated repeatedly to obtain the equilibrated contact angles of the Wenzel and Cassie states.

Characterization. Morphological observation was conducted with a field emission scanning electron microscope (FE-SEM) (Veeco, S-4300) and a transmission electron microscope (TEM) (JEOL, JEM-3011). The atomic force microscopy (AFM) micrographs were obtained using a Hitachi Nanoman instrument. Raman spectroscopy analysis (LabRAM ARAMIS) was carried out to identify the presence of fullerene particles dispersed in the SMP. Microwave was irradiated on the microlens array for 5 min using a microwave machine with a power of 1000 W. The temperature of nanolens array was measured using an infrared thermometer (RayTemp). Mechanical tensile stress experiments were carried out using a universal testing machine. The tensile tests were performed at room temperature (25 °C) at an extension rate of 1 mm/min, and the thermomechanical tests were also conducted to analyze the shape memory properties of the specimens. More details about the cyclic tensile experiments are explained in Supplementary Information. Nanoindentation experiments were performed using a high temperature ultra-nanoindentation tester (UltraNano, CSM). The contact angle of nanolens array was measured using a contact angle meter (Phoenix-300, SEO). Transmittance and reflectance measurements were carried out using a UV-visible spectrometer (PerkinElmer, Lambda 1050) (Supplementary Fig. S10a).

- Kawata, S., Ono, A. & Verma, P. Subwavelength colour imaging with a metallic nanolens. *Nature Photonics* **2**, 438–442 (2008).
- Lee, L. P. & Szema, R. Inspirations from biological optics for advanced photonic systems. *Science* **310**, 1148–1150 (2005).
- Krishna, V., Stevens, N., Koopman, B. & Moudgil, B. Optical heating and rapid transformation of functionalized fullerenes. *Nat Nanotechnol* **5**, 330–334 (2010).
- Chowdhury, I. *et al.* On-chip cooling by superlattice-based thin-film thermoelectrics. *Nat Nanotechnol* **4**, 235–238 (2009).
- Lee, D. J., Kim, H. M., Song, Y. S. & Youn, J. R. Water droplet bouncing and superhydrophobicity induced by multiscale hierarchical nanostructures. *ACS Nano* **6**, 7656–7664 (2012).
- Pernot, G. *et al.* Precise control of thermal conductivity at the nanoscale through individual phonon-scattering barriers. *Nat Mater* **9**, 491–495 (2010).
- Yu, J. K., Mitrovic, S., Tham, D., Varghese, J. & Heath, J. R. Reduction of thermal conductivity in phononic nanomesh structures. *Nat Nanotechnol* **5**, 718–721 (2010).

- Fang, Y. *et al.* Renewing functionalized graphene as electrodes for high-performance supercapacitors. *Adv Mater* **24**, 6348–6355 (2012).
- Xie, T. Tunable polymer multi-shape memory effect. *Nature* **464**, 267–270 (2010).
- Liu, C., Qin, H. & Mather, P. T. Review of progress in shape-memory polymers. *J Mater Chem* **17**, 1543–1558 (2007).
- Rao, C. N. R., Seshadri, R., Govindaraj, A. & Sen, R. Fullerenes, nanotubes, onions and related carbon structures. *Materials Science and Engineering R15*, 209–262 (1995).
- Chopra, S. & Alam, S. Fullerene containing polyurethane nanocomposites for microwave applications. *J Appl Polym Sci* **128**, 2012–2019 (2012).
- Paton, K. R. & Windle, A. H. Efficient microwave energy absorption by carbon nanotubes. *Carbon* **46**, 1935–1941 (2008).
- Yang, D. *et al.* A novel shape memory polynorbornene functionalized with poly(ϵ -caprolactone) side chain and cyano group through ring-opening metathesis polymerization. *Polymer* **51**, 5100–5106 (2010).
- Hu, J. L., Ji, F. L. & Wong, Y. W. Dependency of the shape memory properties of a polyurethane on thermomechanical cyclic conditions. *Polym Int* **54** (2005).
- Koerner, H., Price, G., Pearce, N. A., Alexander, M. & Vaia, R. A. Remotely actuated polymer nanocomposites--stress-recovery of carbon-nanotube-filled thermoplastic elastomers. *Nat Mater* **3**, 115–120 (2004).
- Leng, J., Lan, X., Liu, Y. & Du, S. Shape-memory polymers and their composites: stimulus methods and applications. *Progress in Materials Science* **56**, 1077–1135 (2011).
- Tee, B. C., Wang, C., Allen, R. & Bao, Z. An electrically and mechanically self-healing composite with pressure- and flexion-sensitive properties for electronic skin applications. *Nat Nanotechnol* **7**, 825–832 (2012).
- Yang, B. in School of Mechanical and Aerospace Engineering, Vol. A dissertation for the degree of doctor of philosophy (Nanyang Technological University, Singapore; 2005).
- Wornyo, E., Gall, K., Yang, F. & King, W. Nanoindentation of shape memory polymer network. *Polymer* **48**, 3213–3225 (2007).
- Khanolkar, M. in Department of Mechanical Engineering, Vol. A dissertation for the degree of doctor of philosophy 133 (New Jersey Institute of Technology, 2010).
- Diani, J., Liu, Y. & Gall, K. Finite strain 3D thermoviscoelastic constitutive model for shape memory polymers. *Polym Eng Sci* **46**, 486 (2006).
- Nguyen, T. D., Qi, H. J., Castro, F. & Long, K. N. A thermoviscoelastic model for amorphous shape memory polymers: incorporating structural and stress relaxation. *J Mech Phys Solids* **56**, 2792–2814 (2008).
- Liu, Y. P., Gall, K., Dunn, M. I., Greenberg, A. R. & Diani, J. Thermomechanics of shape memory polymers: uniaxial experiments and constitutive modeling. *Int J Plast* **22**, 279–313 (2006).
- Hu, L. & Chen, G. Analysis of optical absorption in silicon nanowire arrays for photovoltaic applications. *Nano Lett* **7**, 3249–3252 (2007).
- Lee, S. H. et al. Nanocone tip-film solar cells with efficient charge transport. *Adv Mater* **23**, 4381–4385 (2011).
- Zhu, J., Hsu, C. M., Yu, Z., Fan, S. & Cui, Y. Nanodome solar cells with efficient light management and self-cleaning. *Nano Lett* **10**, 1979–1984 (2010).
- Yao, Y. C., Tsai, M. T., Lu, P. W., Wu, C. J. & Lee, Y. J. Effect of nanostructured architecture on the enhanced optical absorption in silicon thin-film solar cells. *Journal of Electromagnetic Waves and Applications* **26**, 1798–1807 (2012).
- Lee, J. Y. *et al.* Near-field focusing and magnification through self-assembled nanoscale spherical lenses. *Nature* **460**, 498–501 (2009).
- Li, W. & Amirfazli, A. A thermodynamic approach for determining the contact angle hysteresis for superhydrophobic surfaces. *J Colloid Interface Sci* **292**, 195–201 (2005).

Acknowledgments

This research was supported by Basic Science Research Program through the National Research Foundation of Korea (NRF) funded by the Ministry of Education, Science and Technology (2013R1A1A2059827). This work was also supported by a National Platform Technology grant (10033636) from the Ministry of Trade, Industry and Energy of Korea.

Author contributions

J.Y.J. and S.J. carried out all the experiments, and J.H.J. and H.B. analyzed the data. J.R.Y. and Y.S.S. designed the system and wrote the paper. All authors reviewed the manuscript.

Additional information

Supplementary information accompanies this paper at <http://www.nature.com/scientificreports>

Competing financial interests: The authors declare no competing financial interests.

How to cite this article: Jeon, S. *et al.* Fullerene Embedded Shape Memory Nanolens Array. *Sci. Rep.* **3**, 3269; DOI:10.1038/srep03269 (2013).



This work is licensed under a Creative Commons Attribution-NonCommercial-ShareAlike 3.0 Unported license. To view a copy of this license, visit <http://creativecommons.org/licenses/by-nc-sa/3.0>